# Measurement of the Absolute Hohlraum-Wall Albedo under Ignition Foot Drive Conditions

O. S. Jones, S. H. Glenzer, L. J. Suter, R. E. Turner, K. M. Campbell, E. L. Dewald, B. A. Hammel, J. H. Hammer, R. L. Kauffman, O. L. Landen, M. D. Rosen, R. J. Wallace, and F. A. Weber

*Lawrence Livermore National Laboratory, Livermore, California 94551, USA*

(Received 26 November 2003; published 5 August 2004)

We present measurements of the absolute albedos of hohlraums made from gold or from high-$Z$ mixtures. The measurements are performed over the range of radiation temperatures (70–100 eV) expected during the foot of an indirect-drive temporally shaped ignition laser pulse, where accurate knowledge of the wall albedo (i.e., soft x-ray wall reemission) is most critical for determining capsule radiation symmetry. We find that the gold albedo agrees well with calculations using the supertransition array opacity model, potentially providing additional margin for inertial confinement fusion ignition.

DOI: 10.1103/PhysRevLett.93.065002 PACS numbers: 52.57.–z

Indirect drive inertial confinement fusion uses high intensity lasers or particle beams to heat a high-$Z$ cavity (hohlraum) that produces soft x rays characterized by a radiation temperature $T_{\mathrm{RAD}}$ [1]. The x rays heat and ablate the surface of a DT-filled fusion capsule, compressing and heating the DT fuel until it ignites. Current indirect drive target designs predict that ignition and gain can be achieved by heating hohlraums with a temporally shaped 1.5–2 MJ, 0.35 $\mu$m laser pulse [2]. The baseline National Ignition Facility (NIF) ignition target laser pulse creates a time-dependent $T_{\mathrm{RAD}}$, or "drive," that consists of a 10 ns long "foot" at 80–100 eV, followed by a rapid increase in $T_{\mathrm{RAD}}$ to a peak of 300 eV at 15 ns. It is important that the radiation drive onto the capsule be as symmetric as possible during the foot (as well as during the rest of the pulse) in order to efficiently compress the DT fuel.

The albedo is the ratio of the reemitted x-ray flux to the incident x-ray flux. Accurate knowledge of this quantity is important to the ignition effort because it affects our estimates of the asymmetry during the foot. Radiation uniformity depends on a variety of parameters including the location of the laser spots on the hohlraum wall and the x-ray brightness of those spots relative to the soft x-ray reemission from the unirradiated wall. Higher albedo leads to a larger ratio of wall reemission to spot brightness, which reduces capsule asymmetries due to laser power imbalance and beam mispointing.

In this Letter, we report on experiments that measure the absolute albedo of hohlraums made from several different high-$Z$ materials at radiation temperatures close to the NIF foot radiation temperature. There have been many previous investigations of reemission from laser heated hohlraums [3]. However, in our experiment the high-$Z$ hohlraum from which we infer the albedo is heated by x rays from an attached hohlraum and not directly by a laser, thus eliminating x-ray conversion efficiency and laser backscatter as parameters in the data analysis [4]. In this regard, this work is similar to previous $z$-pinch-driven hohlraum experiments [5]. Moreover, in our experiment the same instrument measures the flux incident upon the high-$Z$ hohlraum wall and the flux reemitted from the wall. This technique results in a measurement error in the albedo of only $\pm 0.06$. We show that the albedo of gold inferred from the experiment matches well with predictions using the radiation hydrodynamics code LASNEX [6], with opacities from the supertransition array (STA) model [7,8]. The measured albedo is larger than predicted from calculations that use the average-atom cross-section (XSN) model [9] for the opacity. This is important because the original NIF laser power balance specifications [10] were based on modeling of gold hohlraums that used the average-atom XSN approximation for the opacities, resulting in an albedo at the end of the 10 ns, 80 eV foot pulse that is ~20% lower than predicted using STA opacities. Figure 1 shows the

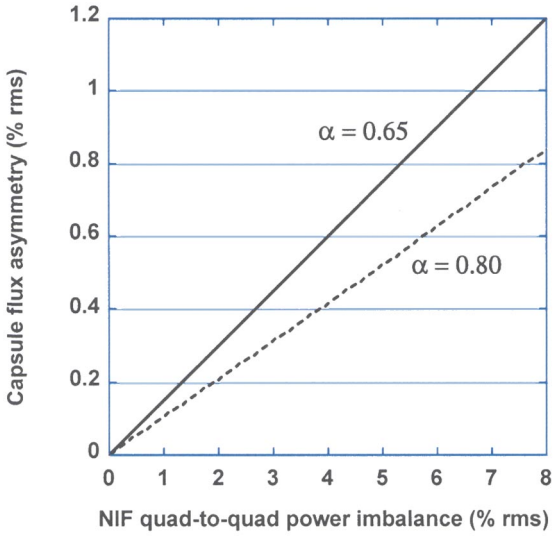


FIG. 1 (color online). Flux asymmetry onto ignition capsule during foot of pulse as function of random quad-to-quad (quad = 4 beams) laser power imbalance and wall albedo.

 0031-9007/04/93(6)/065002(4)$22.50  

variation in the random component of the flux asymmetry onto an ignition capsule during the foot as a function of the random laser power imbalance and the wall albedo. The curve for the albedo of 0.65, which is consistent with XSN estimates of the average albedo for a gold hohlraum during the foot of an ignition pulse, is taken directly from Ref. [10]. The allowable contribution from laser imbalance to the flux asymmetry during the foot is about 0.6% rms, which corresponds to a foot-averaged quad-to-quad imbalance of about 4% rms, and is consistent with the NIF specification. The other curve is for a wall albedo of 0.80, which is more representative of the average wall albedo estimated using STA opacities. We see that at an albedo of 0.80 the radiation on the capsule should be ~30% more uniform than previously estimated, providing an additional margin for ignition.

The experiments to measure low $T_{\mathrm{RAD}}$ albedo were performed at the Omega laser facility. The basic configuration [Fig. 2(b)] consisted of two attached hohlraums. The primary hohlraum (1600 $\mu$m diameter, 1125 $\mu$m length) produced the x-ray drive that heated the secondary hohlraum, whose wall reemission was measured in order to infer the wall albedo. The primary hohlraum was heated by 15 beams entering from one side that delivered

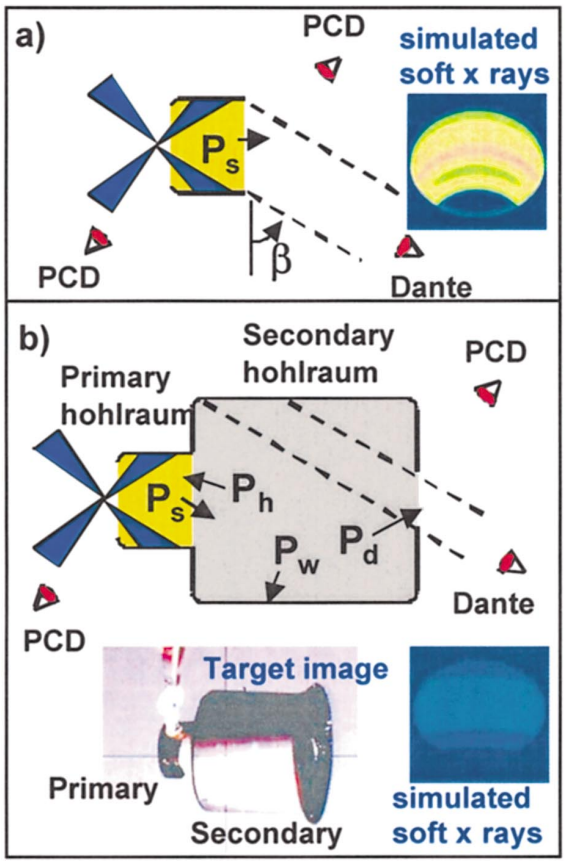


FIG. 2 (color). Schematic of the (a) primary and (b) double hohlraum experiment together with x-ray power diagnostics and calculated x-ray emission.

6.5 kJ in a 1.5 ns temporally flat pulse. It reached a peak radiation temperature of ~160 eV and that radiation heated the larger secondary hohlraum. We tested secondary hohlraums (with 3440 $\mu$m diameter and 3750 $\mu$m length) made of gold, uranium (alloyed with 14% atomic fraction niobium), and a mixture (or "cocktail") [11–13] made up of 52% uranium, 8% niobium, 20% gold, and 20% dysprosium. These secondary hohlraums reached a peak radiation temperature of ~100 eV. We also tested a larger gold secondary hohlraum (with 4400 $\mu$m diameter and 4800 $\mu$m length), which peaked at ~70 eV.

The radiation power out of the secondary hohlraum's 1000 $\mu$m diagnostic hole ($P_d$) was measured by the Dante filtered x-ray diode (XRD) array [14] and also by a photoconductive detector [15]. The total radiation power per solid angle was obtained from the multichannel XRD by convolving a trial spectrum with the channel response functions to get computed channel signals and then iterating the spectrum until the computed signals approximately match the measured signals for each channel. To directly measure the power leaving the primary hohlraum and heating the secondary hohlraum (the radiation source power $P_s$), we also shot the primary hohlraum without the secondary attached [Fig. 2(a)], so that the power from the primary ($P_s$) could be measured with the same two instruments as $P_d$. The principal measurement from this experiment is the ratio of the radiation power per solid angle exiting the primary hohlraum to the radiation power per solid angle exiting the secondary hohlraum. We now show that this ratio depends on the albedo of the secondary hohlraum wall.

A radiation power balance model [16] for the secondary hohlraum can be formulated as

$$P_s = P_h + P_d + P_w, \tag{1}$$

where $P_s$ is the source radiation power coming from the primary hohlraum, and $P_h$, $P_d$, and $P_w$ are the radiation sinks leaving the secondary hohlraum through the hole between the two hohlraums, through the diagnostic hole, and into the wall, respectively (see Fig. 2). The source spectrum is slightly non-Planckian due to the $M$-band radiation from the laser spots (intensity at wall $\sim 10^{16}$ W/cm$^2$, ~10 times higher than expected NIF wall intensities). However, for gold at 100 eV, the albedo is not sensitive to the spectrum except for the first ~100 ps, when the mean free path is greater than or equal to the penetration depth of the radiation heat wave [1]. We define the average radiation temperature in the secondary hohlraum, $T_{\mathrm{RAD}}$, by equating the total frequency-integrated radiation flux inside the hohlraum to a blackbody flux $\sigma T_{\mathrm{RAD}}^4$, where $\sigma$ is the Stefan-Boltzmann constant. The radiation power leaving the secondary through holes ($P_h$ and $P_d$) is simply the radiation flux inside the secondary ($\sigma T_{\mathrm{RAD}}^4$) times the hole areas ($A_h$ and $A_d$), respectively. The remaining term $P_w$ is

the radiation power absorbed by the wall. We define the albedo $\alpha$ as the ratio of the emitted radiation flux ($F_{\text{out}}$) to the incident radiation flux ($F_{\text{in}}$). Since the flux reemitted by the wall is proportional to $\alpha$, the radiation power absorbed by the wall is $(1-\alpha)$ times the wall area ($A_w$). When $P_h$, $P_d$, and $P_w$ are expressed in terms of $T_{\text{RAD}}$ and $\alpha$ and substituted into Eq. (1), we find that

$$P_s = \sigma T_{\text{RAD}}^4 [A_h + A_d + A_w(1-\alpha)]. \quad (2)$$

The radiation temperature of the secondary hohlraum ($T_{\text{RAD}}$) in Eq. (2) is inferred from the measured power per steradian from the secondary hohlraum ($P_{\text{XRD2}}$) by noting that the XRD measures the reemitted flux from the secondary wall, whereas $\sigma T_{\text{RAD}}^4$ in Eq. (2) is the flux incident on the wall, related to the reemitted flux via the albedo. We can express the reemitted flux as

$$\alpha\sigma T_{\text{RAD}}^4 = \alpha F_{\text{in,avg}} = \frac{1}{C_2}\alpha F_{\text{in,view}} = \frac{1}{C_2}\frac{P_{\text{XRD2}}\pi}{A_d \sin\beta}, \quad (3)$$

where $\beta$ is the XRD view angle relative to the wall normal (see Fig. 2), $F_{\text{in,avg}}$ is the average incident flux over the entire secondary hohlraum wall ($A_w$), $F_{\text{in,view}}$ is the incident flux over the portion of the secondary hohlraum wall viewed by the XRD, and $C_2$ is the factor that corrects for the nonuniformity of the incident flux. We calculated the spatial variation of the incident flux using a radiation viewfactor code and found that $C_2(\alpha) = 1.927 - 0.834\alpha - 0.065\alpha^2$ for the 3440 $\mu$m (100 eV) secondary and $C_2(\alpha) = 2.044 - 0.946\alpha - 0.080\alpha^2$ for the 4400 $\mu$m (70 eV) secondary.

The total source power ($P_s$) is related to the power per steradian measured by the XRD in the primary-hohlraum shot ($P_{\text{XRD1}}$) by

$$P_s = C_1 P_{\text{XRD1}} \frac{\pi}{\sin\beta}, \quad (4)$$

where $C_1$ is a factor that accounts for the angle dependence of the emission. Here we neglect the small contribution ($< 5\%$) to the source power from the radiation coming back from the secondary hohlraum. From a LASNEX calculation of the gold primary hohlraum, we find that $C_1 = 1$ from 0 to 0.5 ns, varies linearly between 1 and 0.88 from 0.5 to 1.5 ns, and then varies linearly between 0.88 to 0.85 from 1.5 to 2.0 ns. Radiation viewfactor calculations corroborate this result and show that the time dependence is primarily a geometrical effect due to the changing location of the laser absorption region as the hohlraum wall blow-off plasma expands.

Substituting Eqs. (3) and (4) into (2), we get the following equation relating the albedo to the experimentally measured quantities:

$$\frac{P_{\text{XRD2}}}{P_{\text{XRD1}}} = \frac{\alpha C_1(t) C_2(\alpha)}{[1 + \frac{A_h}{A_d} + \frac{A_w}{A_d}(1-\alpha)]}. \quad (5)$$

Figure 3 shows the secondary-to-primary XRD power ratio as a function of time for a 3440 $\mu$m diameter gold secondary hohlraum. The data have 20% error bars, which is the estimated $3\sigma$ uncertainty in unfolding the absolute radiation per solid angle from the ten channel XRD array. The curves are created from the ratio of synthetic XRD powers per solid angle extracted from two LASNEX calculations: a primary-only calculation and a double hohlraum calculation. For one calculation STA opacities are used for the secondary hohlraum, leading to the upper curve which agrees well with the

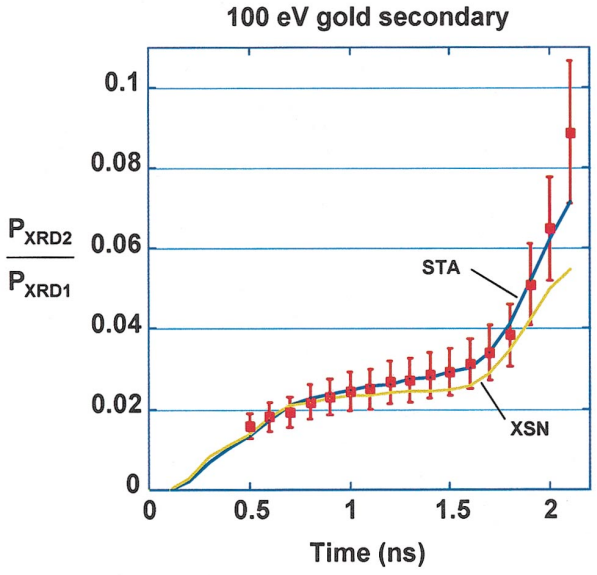


FIG. 3 (color). Measured (squares) and calculated (curves) time-dependent secondary-to-primary power ratio for a 3440 $\mu$m diameter gold secondary hohlraum.

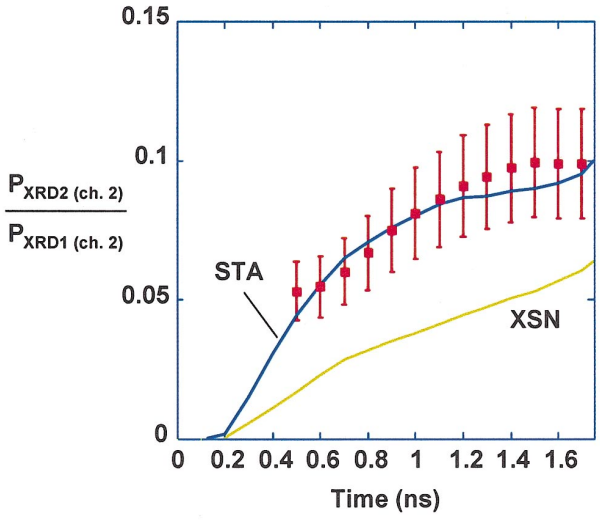


FIG. 4 (color). Measured and predicted ratios of the secondary hohlraum XRD channel 2 (200–280 eV) signal to the primary XRD channel 2 signal.

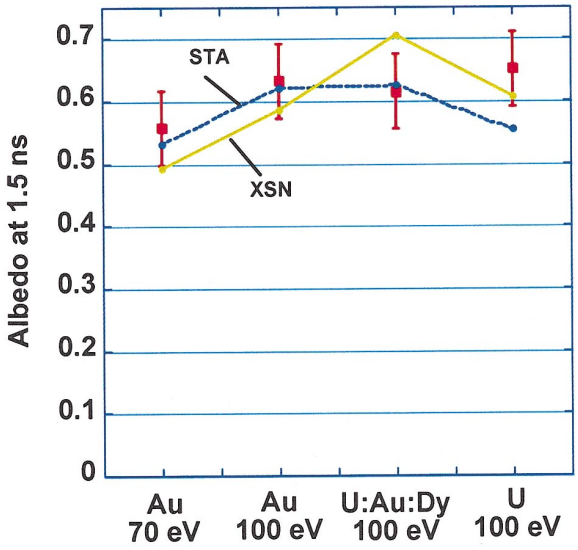


FIG. 5 (color). Comparison of the measured (squares) and predicted hohlraum albedos at peak $T_{RAD}$ for different secondary hohlraums.

data. The lower curve is from an almost identical set of calculations, except that XSN opacities are used in the secondary. The STA curve agrees well with the measurements, whereas the XSN curve generally lies below the measurements and by 2 ns; the probability that the XSN curve agrees with the data is less than 0.04%.

A clearer distinction between the STA and XSN opacity models for gold can be seen by comparing the secondary-to-primary ratios of a single XRD channel rather than comparing the total power ratios obtained from a spectral deconvolution of all ten XRD channels. Rosen [17] has previously shown the inaccuracy of the XSN opacity model for gold at 70–100 eV by examining burn-through measurements. He noted that the inaccuracy is attributable to the lack of $n = 4$ to $n = 4$ transitions near photon energies of 200–300 eV in the XSN average atom approximation. These transitions are included in the more detailed STA opacity model. The second XRD channel covers this important spectral range near the Planckian peak, from ~200–280 eV. Figure 4 compares the measured and calculated XRD channel 2 signal ratios (secondary to primary) for the 100 eV gold secondary hohlraum. The ratio extracted from the STA calculation agrees with the data and is a factor of 2 above the XSN value, providing clear experimental verification that STA is needed to accurately model gold at this radiation temperature.

The data for all hohlraum materials are plotted (Fig. 5) in terms of an equivalent albedo at peak $T_{RAD}$ ($t = 1.5$ ns) by substituting the secondary-to-primary XRD power ratio into Eq. (5). The measured albedos are known to within $\pm 0.06$, which follows from Eq. (5), assuming a 20% uncertainty in the measured secondary-to-primary XRD ratio and neglecting any additional uncertainty in $C_1$, $C_2$, and diagnostic hole closure. The measured albedos are compared to the predicted albedos from the simulations that used STA or XSN opacities in the secondary hohlraum. The predicted albedos are also obtained from Eq. (5) but using the simulated secondary-to-primary XRD ratio instead of the measured ratio. For the gold and cocktail hohlraums, we see good agreement between the data and the STA prediction. For the gold hohlraums, the XSN prediction lies below the measurements. There is a probability of 0.1% (2.5%) that the XSN model is in agreement with the 70 eV (100 eV) gold hohlraum measurements. We note here that the cocktail hohlraum does not have a higher albedo than gold at 100 eV because the mixture of materials was chosen to maximize the albedo for radiation temperatures of 250–300 eV that occur during the peak of the ignition drive pulse. Only the uranium hohlraum albedo disagrees with the STA prediction, suggesting a possible area for further research.

In summary, we have performed absolute measurements of the albedo of high-$Z$ hohlraums in the temperature range of 70–100 eV, which is the range of temperatures that characterize the foot of an indirect drive ignition pulse. We find that the albedo of gold predicted from LASNEX calculations that use the STA opacity model agree well with the measured values and that calculations using STA opacities provide better overall agreement with the data than calculations that use the average atom XSN model for the opacity.

[1] J. Lindl, *Inertial Confinement Fusion* (Springer-Verlag, New York, 1998).
[2] S. W. Haan *et al.*, Phys. Plasmas **2**, 2480 (1995).
[3] H. Nishimura *et al.*, Phys. Rev. A **44**, 8323 (1991); I. B. Foldes *et al.*, Phys. Rev. E **50**, R690 (1994).
[4] S. H. Glenzer *et al.*, Phys. Rev. Lett. **80**, 2845 (1998).
[5] R. E. Olson *et al.*, Rev. Sci. Instrum. **72**, 1214 (2001); T. W. L. Sanford *et al.*, Phys. Rev. Lett. **83**, 5511 (1999).
[6] G. B. Zimmerman and W. L. Kruer, Comments Plasma Phys. Controlled Fusion **2**, 51 (1975).
[7] A. Bar-Shalom *et al.*, Phys. Rev. A **40**, 3183 (1989).
[8] M. Klapisch *et al.*, Phys. Plasmas **8**, 1817 (2001).
[9] D. E. Post *et al.*, At. Data Nucl. Data Tables **20**, 397 (1977).
[10] J. D. Lindl *et al.*, Phys. Plasmas **11**, 339 (2004).
[11] H. Nishimura *et al.*, Appl. Phys. Lett. **62**, 1344 (1993).
[12] T. J. Orzechowski *et al.*, Phys. Rev. Lett. **77**, 3545 (1996).
[13] D. Colombant, M. Klapisch, and A. Bar-Shalom, Phys. Rev. E **57**, 3411 (1998).
[14] H. N. Kornblum and R. L. Kauffman, Rev. Sci. Instrum. **57**, 2179 (1986).
[15] R. E. Turner *et al.*, Rev. Sci. Instrum. **70**, 656 (1999).
[16] L. Suter *et al.*, Phys. Plasmas **3**, 2057 (1996).
[17] M. D. Rosen, Phys. Plasmas **3**, 1803 (1996).